Validating and Modeling of Steam Turbine Temperature Distribution for Different Operational Cases

Sebastian Sporre

LUNDS UNIVERSITET

Thesis for the Degree of Master of Science

Thesis Advisor: Magnus Genrup and Oskar Mazur

Thesis Examiner: Marcus Thern

"I've believed in the Toronto Maple Leafs my entire life. The least you could do is believe in yourself"

Steve Dangle Glynn

This thesis for the degree of Master of Science in Engineering has been conducted at the Division of Thermal Power Engineering, Department of Energy Sciences, Lunds Tekniska Högskola (LTH) – Lund University (LU) and at Siemens Industrial Turbomachinery AB (SIT AB).

Supervisor at SIT AB: Oskar Mazur;
Supervisor at LU-LTH: Professor Magnus Genrup;
Examiner at LU-LTH: Associate Professor Marcus Thern.

Abstract

Collective solar power, with its uncertain power availability, requires an increasing amount of flexibility to operate optimally. Thermal stress in thick-walled parts, such as the rotor and casing, limits the rate of which hot steam can be entered into the turbine. Precise knowledge of the thermal stress in these components is crucial to utilise as much of the available power as possible. The Steam Turbine Thermal Transient Model (ST3M) tool developed at KTH does precisely that, it's a 2D FE tool that calculates the temperature distribution and thermal stress in a modular turbine geometry. In this thesis three different operating cases where studied to investigate the tools usability. The three cases where a normal day's operation with a long cool-down, a full speed, no load case (FSNL) and lastly the effect of a sudden load drop with the subsequent ramping up. ST3M was found to following load changes well, with some required manual adjustment, but was not able to follow the long cool-down and the FSNL case was not able to replicate the real world operation.

Nomenclature

Abbreviations

CSP	Collective Solar Power
FE	Finite element (method)
FSNL	Full speed, no load
HP	High pressure (turbine)
HTC	Heat transfer coefficient
IP	Intermediate pressure (turbine)
LCF	Low cycle fatigue
LP	Low pressure (turbine)
ST3M	Steam Turbine Thermal Transient Model
TSE	Thermal stress evaluator

Latin Symbols

d_s	Seal diameter	$[m]$
E	Youngs modulus	$[MPa]$
h	Enthalpy	$[kJ/kgK]$
k	Heat conductivity	$[W/mK]$
$\dot{m}$	Mass flow	$[kg/s]$
N	Revolutions per second	$[1/s]$
Nu	Nusselt number	$[-]$
P	Pressure	$[bar]$
Pr	Prandtl number	$[-]$
Re	Reynolds number	$[-]$
T	Temperature	$[\deg C]$
t_ins	Insulating thickness	$[mm]$
u	Circumferential speed	$[m/s]$
W	Work	$[W]$
z	Number of teeth	$[-]$

Greek Symbols

α	Thermal expansion coefficient	$[-]$
β_2	Blade outlet angle	$[deg]$
δ	Seal radial clearance	$[mm]$
η	Efficiency	$[-]$
λ	Tooth width	$[mm]$
ν	Poisson's ratio	[-]
	Specific Volume	$[m^3/kg]$
ρ	Density	$[kg/m^3]$
σ_T	Thermal stress	$[Pa]$
τ	Tooth pitch	$[mm]$
Φ	Mass flow coefficient	$[-]$

Contents

Chapter 1

Introduction

Todays energy market requires more and more flexible generation, both heat and electricity. This is especially true for collective solar power, where at least one startup of the turbine is required each day but it is also true for previously baseload plants that now has been forced into more and more cyclical use due to the penetration of intermittent renewable energy sources. Thermal stress in thick-walled components is the most limiting factor to allow for faster start-ups, this demands greater and greater knowledge from the turbine manufacturer to be confident in pushing the limits of the turbines. Accurate knowledge of the exact thermal stress in the turbine is critical to maximize the usage of the turbine during its lifetime and the tools to analyze this is of much importance. The Concentrating Solar Power and Techno-Economic Analysis Group as a part of the Department of Energy at KTH has developed a tool for just that, called ST3M. This is a MATLAB based code that utilizes the multi-physics program COMSOL to create a 2D axissymmetric model of a turbine in order to calculate the thermo-mechanic properties of the modeled turbine.

This was used to run three different cases of operation:

1. Operation during one day based on measured inlet data with a cool-down equal to one weekend
2. A unique case where the mass flow unintentionally was restricted and heat was generated due to friction and ventilation
3. The effect of sudden load drops associated with clouds in solar power plants

All the cases studied were based on the same high pressure turbine and therefore the geometrical modeling aspect of the code was not studied, the geometry of the turbine was provided by previously completed studies. In all three cases the heat transfer coefficients were calculated with the built-in theoretical equations found in literature, however the tool is equipped to handle pre-determined heat transfer coefficients from manufacturers. The boundary conditions was fairly similar for the first and third case, with the most common thermal boundary condition being that of convection. However for the second case where no live steam was introduced, no convection can occur and radiation instead took its place.

1.1 Objectives

The objectives for this master thesis is to:

- Validate ST3M against operational data and Full Speed, No load case
- Calculate temperature differences in major components during sudden load drop and subsequent ramping
- Evaluate industrial usefulness of the ST3M code

The first to cases was run as validating cases, while the second one presented results to the industry for evaluation. However due to the time-line of this thesis, there was not enough time in this thesis or by Siemens to fully evaluate the results. The industrial usefulnesses was evaluated throughout the thesis gathered from the experience with using the tool.

Chapter 2

Theory

2.1 Steam turbine fundamentals

We classify turbo machines as a device that transfers energy either to or from a continuously flowing fluid. This is a rather large field of machines that stretches to everything from your ordinary desk fan, to pumps, to wind power plants and to steam turbines which will be the focus of this thesis. [1]

In its most basic form a steam power plant is essentially a large water boiler, driven by some kind of fuel where coal and biofuel are very common ones, coupled to one or several turbines that in turn are coupled to an electric generator. Water is evaporated into steam in the boiler and then injected into the turbines where there are several sets of stationary and rotating blades which can extract work from the steam to rotate the central rotor connected to each turbine as well as the electric generator. The generator can then produce electricity and with the addition of heat exchangers the spare heat can be used for district heating as well.

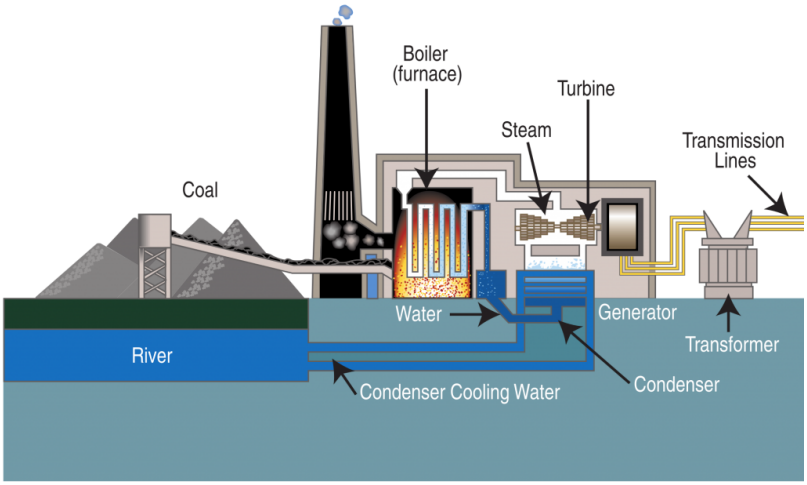

Figure 2.1: Simplified layout of a steam power plant[2]

The thermal process of a steam turbine is called the Rankine cycle and is most easily displayed in a temperature-entropy diagram, or t-s digram. This shows the temperature on the y axis and the entropy on the x axis. The bell-shaped curve indicates phase shifts of water, to the left the water is liquid, to the right its superheated steam and under the curve the water is saturated liquid-vapor. The four steps in the rankine cycle are:

1. The liquid water is pumped to a higher pressure
2. The now high pressure liquid water enters the boiler and heat is added by an external source to the point of either a dry saturated vapor or a superheated vapor
3. The vapor enters the turbine where work is extracted and thusly the temperature and pressure lowered
4. The saturated water enters the condenser where it is condensed to become a fully saturated liquid.

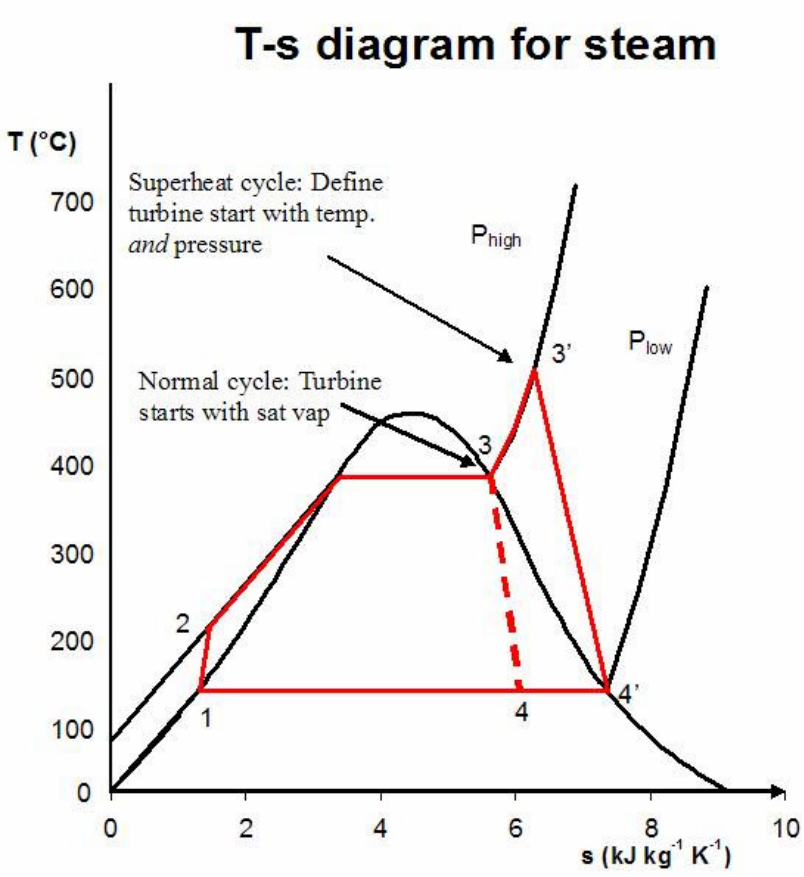

Figure 2.2: Rankine cycle with overheat

2.2 Thermal stress

There is an ever-growing demand on steam turbines' flexibility, their ability to start quicker and handle faster load change rates. What has traditionally limited a faster start-up is the increased thermal stress that would occur due to inducing a high temperature difference. Start-ups in turbines are usually categorized in three temperature regions:

- Cold starts with an outage of more than 72 hours or a metal temperature not exceeding 160°C
- Warm starts with an outage of between 10-72 hours or metal temperature between 160-400°C
- Hot starts with an outage of less than 10 hours or a metal temperature exceeding 400°C

There is also something called ambient starts which is exceedingly rare and occurs after a major outage or when the metal temperature is below 50°C. Hot starts are often associated with the turbine being turned off during the night for non-baseload plants, while warm starts is associated with being turned off over the weekend. To stay within the allowed range of thermal stresses the cold starts takes the longest time with about 75-150 minutes for a 450 MW combined cycle plant, 75-110 minutes for warm starts and 40-50 minutes for hot starts.[3]

The importance of the difference in metal temperature in the turbine is because of the source of thermal stresses, which can be found to be proportional to the temperature difference over the thick-walled parts of the turbine. During operation the rotor of the turbine will heat up to a temperature roughly equal to the inlet steam temperature at the inlet side of the rotor, when the turbine trips or is unloaded the rotor will cool down. When steam then is reintroduced during start-up the difference between the hot inlet steam and the now cooled off rotor will cause high thermal stresses in the metal of the rotor. The same happens in the thick walls of the turbine casing which is often seen as the main limiting components in regards to turbine start-ups. [4]

Looking at the turbine casing subjected to a temperature gradient, the casing will be subjected to thermal expansion and therefore tension where the temperature is higher than the mean temperature, and compression where the temperature is below the mean. This is what causes the thermal strain.

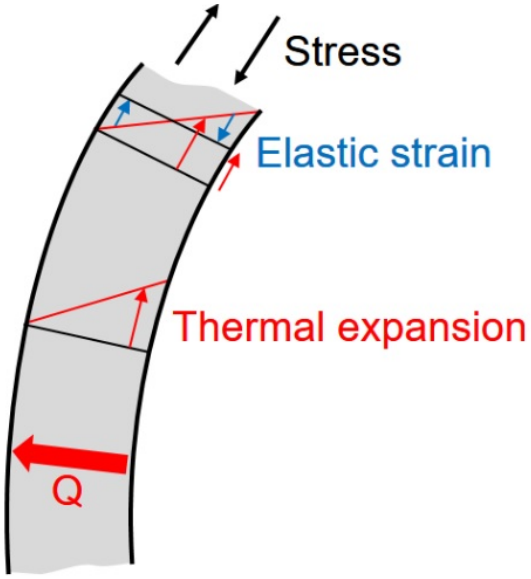

Figure 2.3: Thermal strain[5]

If the casing is seen as thin-walled, the induced temperature difference can be translated to thermal stresses with equation 2.1. However this is a simplification compared to reality and for more accurate calculations finite element calculations are applied.[5]

$$\sigma_T = \frac{\alpha * E}{1 - \nu} \Delta T \tag{2.1}$$

Where σ_T is the induced thermal stresses and ΔT is the temperature difference. α is the thermal expansion coefficient, ν is the Poisson's ratio and E is the elasticity module and are all material properties. This means that a higher starting temperature of the thick-walled components will, for the acceptable thermal stress, allow for a higher temperature of the inlet steam. The closer the temperature of the inlet steam is to the nominal value the shorter the startup time will become.

The thermal stresses generated will unavoidably consume the lifetime of the turbine and will in the end always lead to cracks and eventually failure. Due to the lifetime of the turbine and the expected number of starts this is usually categorized as low cycle fatigue (LCF), which is defined as a component failing due to repetitive stresses in less than 100 000 cycles.[4] Depending on the intended usage, the startup can be designed to be more aggressive and in turn consume more lifetime per start. However the lifetime is designed, the thermal stresses introduced in the turbine will cause performance deterioration before reaching the end of the lifetime. The efficiency of the turbine will slowly deteriorate caused by several factors, one example being an increased leakage in the steam path caused by rubbing of the seals.

When converting thermal stresses to consumption in life time one of the simplest and

most straight-forward models is the Palmgren-Miner's rule, which is a cumulative damage model:

$$\sum_{i=1}^{k} \frac{n_i}{N_i} = 1 \tag{2.2}$$

It states that there are k number of different stress levels, N_i is the average number of cycles until failure at a specific stress level and n_i is the number of cycles accumulated at this stress level, when the total sum of all fractions reaches 1 failure will occur. For example, if it is known that a component will fail after 500 cycles at 10 MPa, we know that after 250 cycles at 10 MPa half of the lifetime has been consumed. If the stress is instead reduced to 5 MPa from 10 MPa, according to Palmgren-Miner failure will occur at 1000 cycles instead. If half the lifetime has been consumed by running 250 cycles at 10 MPa, only 500 cycles at 5 MPa is needed to reach failure.[6]

2.3 Start-up curves

Depending on the designed number of starts certain thermal stresses and in turn temperature differences are allowed. The measure with which the manufacturers of turbines control the allowed range is start-up curves, which typically defines the rotational speed of the rotor, the inlet pressure, temperature and the subsequent power produced. A typical start-up curve is shown in figure 2.4. To be noted is that this would be just one of many start-up curves for one specific turbine, there would be several start-up curves for each starting state (cold, warm, hot) for each specific steam turbine. Since there is however a finite amount of startup curves, they are a compromise of sorts. There is not one startup curve for every single temperature, but instead one specific curve covers a span of temperatures. If the actual temperature is in the lower end of of this span, the curve is in reality over-conservative and isn't utilizing the full potential of the acceptable thermal stress. This means the turbine is starting slower than it has too and takes longer to reach nominal power, which means the operator stands to lose potential profit.

One technology to help do away with the old system of start-up curves are thermal stress evaluators (TSE) which measures the temperature of the casing and a non-rotating point in close proximity to the rotor directly. The temperature in the rotor is calculated from the second measurement and heat conduction equations. The TSE can then directly control the turbine to stay close to, but under the allowed temperature range. This technology would render the start-up curves obsolete for all types of starts, except as last resort backups. As a result of introducing TSE not only would it always utilize the full potential during every start, it would also open up opportunities to give the operator more control over the time needed for the start-up with the choice of several start-up speeds but at the cost of more lifetime consumption per start. This would present the option of a normal, fast, faster start with the

fast and faster starts being designed more aggressively so as to exceed the previously allowed temperature differences and consequently consume more lifetime.[3]

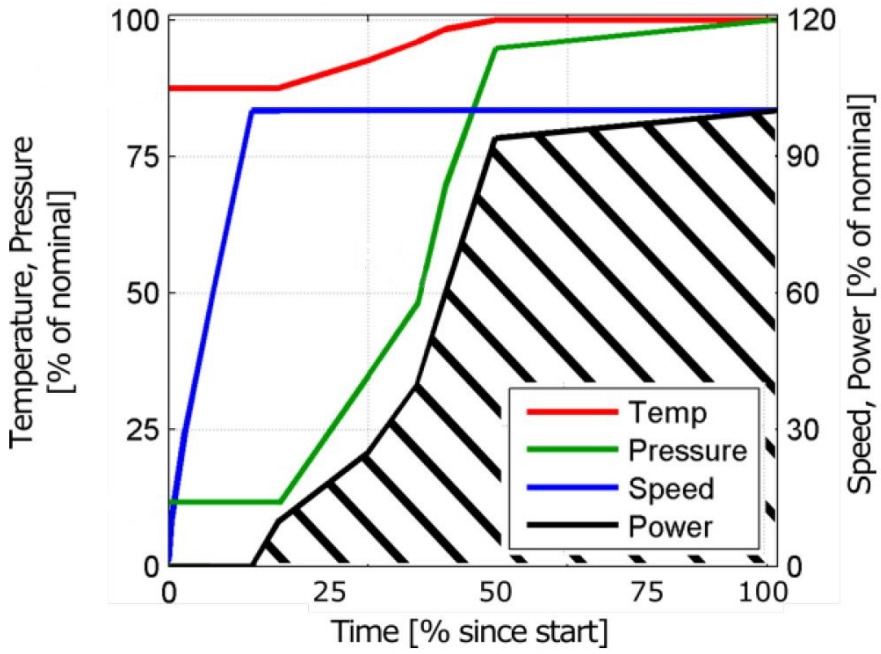

Figure 2.4: Start-up curve
[7]

2.4 Thermal Expansion

While the start-up curves are designed to limit the thermal stresses in the thick-walled components in the turbine, if the option for faster, more lifetime-consuming starts were to be introduced the phenomena of thermal expansion could become the leading limiting factor instead. The linear thermal expansion can be calculated with:

$$\Delta L = L_0 \cdot \alpha \cdot (T - T_0) \tag{2.3}$$

Where ΔL is the length expansion of the object, L_0 is the original length of the object, α is the thermal expansion coefficient, T and T_0 is the final and starting temperature respectively. This is however only the expansion in one dimension and only holds true if the expansion coefficient is fairly constant over the temperature change.

Whilst unhindered thermal expansion does not cause any stresses in the material, if the rotating parts and stationary parts were to expand differently, rubbing might occur if the axial

and radial clearances are not large enough. This would reduce the lifetime of the components experiencing the rubbing and could quickly lead to machine failure. While today turbine manufacturers set clearances large enough to handle the thermal expansion caused by the thermal gradients during start-up operation, an introduction of more aggressive start-ups might cause rubbing in the pre-existing turbines with already set clearances. This would not be a problem for newly produced turbines designed for this new technology though, since the clearances can be set to handle the faster start-ups. Whether or not this relative expansion will create problems is not a well researched topic although some studies have shown it might cause problems. [8]

2.5 Concentrated solar power plants

Concentrated solar power (CSP) is one of the more promising technologies to provide renewable electricity today and in the future. With many commercialized plants around the world, primarily in Spain and the US, the technology is already fully operational but as a rather new technology there is big potential for more improvement. CSP works just as the name suggests by concentrating the power of the sun. The sun's rays are redirected and concentrated by mirrors and heats up a fluid medium which is then used to power a classic steam turbine Rankine cycle. The two most common mirror-setups is either a so called parabolic trough or a solar tower, with the first seen as the more mature one and the latter as the one with the most future potential. There is also two additional types called parabolic dish and linear Fresnel which works similarly as the previous two but is not as common. [7]

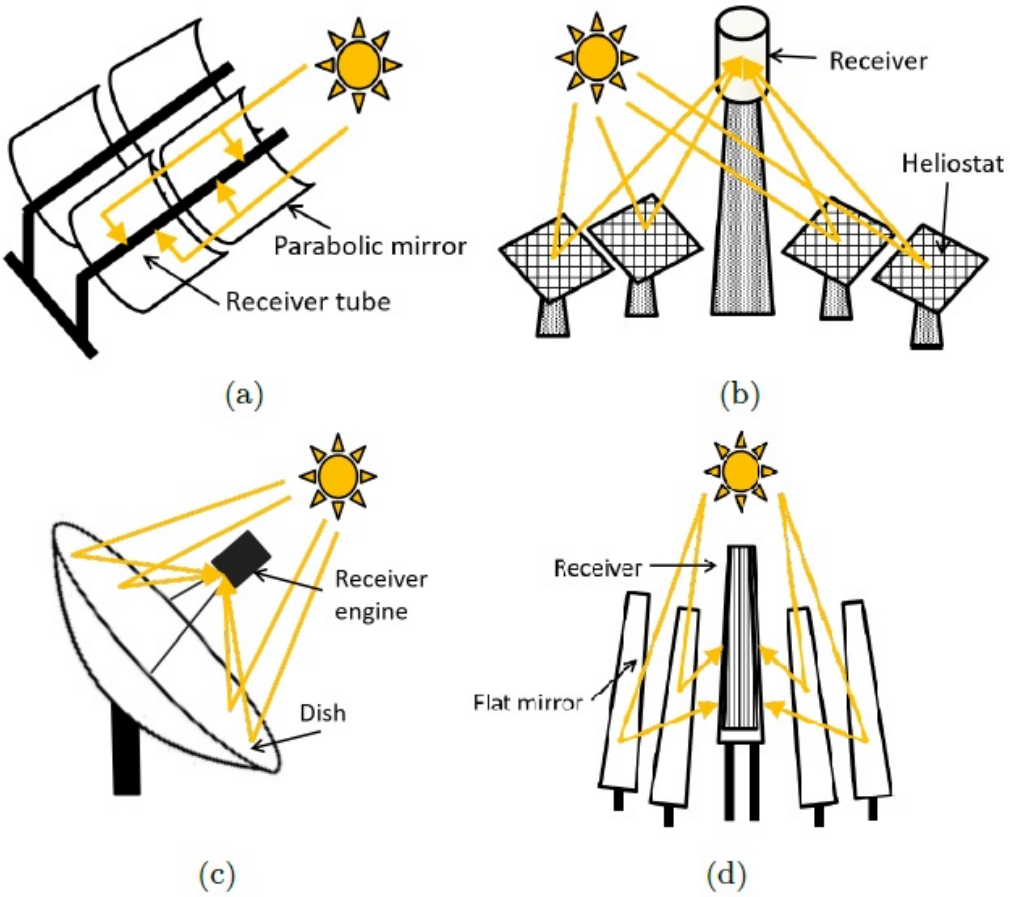

Figure 2.5
(a) Parabolic Trough (b)Power Tower (c) Parabolic Dish (d) Linear Fresnel[7]

Solar towers due to their higher concentration factor, can reach higher temperature compared to parabolic trough. Higher temperature is fundamental to increase the efficiency of a Rankine cycle and is the main point why the tower-setup is considered as having more potential for development in the future.[7] There are essentially two types of heat transfer fluids in a tower setup, molten salt and direct steam generation in the solar receiver at the top of the tower. The direct steam method offers a simpler plant design with the steam from the central receiver going directly to the power block. In the case of heated molten salt the heat is exchanged to the steam turbine cycle but first is usually passed through tanks for thermal energy storage, one of the biggest advantages with using molten salts. One of the most famous CSP installations, Solar One which was later reconfigured into Solar Two, utilized this technique by directing all of the heated salt directly into the storage and drawing heat from the storage to power the

turbine. This decouples the heat generation from the electricity generation which provides higher availability of electricity. [9] Today typical storage sizes are about 8-12 hours to cover the production during nighttime.[7]

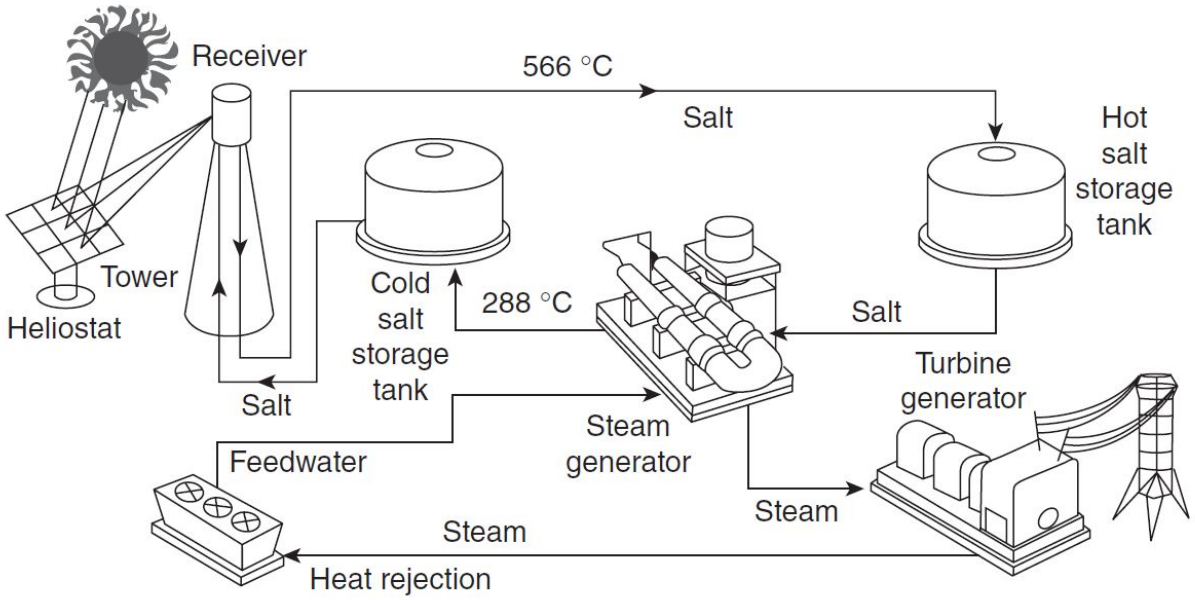

Figure 2.6
Solar Two setup with two tank molten-salt storage.[9]

The largest CSP plant in operation today is the Ivanpah Solar Facility, it has a gross capacity of 392 MW. It has a direct steam configuration with no storage powered by a Siemens SST-900 steam turbine and consists of 173 500 heliostats with two mirrors on each heliostats. It is located outside the town of Primm in California, close to the state border to Nevada.[10]

Figure 2.7
Ivanpah Solar Power Plant.[11]

CSP operation is a heavy cyclical one, with startup and shutdown at least once every day, compared to a few times a year for large base-load plants. In the base-load combined cycle plants the loading rates and main steam parameters are all controllable and can be kept under the allowed maximum limit, this is not possible in the same way for a weather dependent solar tower plant. Modern steam turbines can handle cycling operation relatively well but it's still one of the most intricate parts of turbine operation and will need further development and adaption to CSP-specific usage.[12]

2.6 Flexibility

With the introduction of an increasing penetration of intermittent renewable energy sources the future need for steam turbines ability to adapt for more flexible operation will increase as well. While steam turbines has historically been used for base load operation, the non-dispatchability of solar and wind energy production forces steam turbine to enter more cyclical operation. This is due both to the usage of steam turbines in concentrated solar plants which is highly cyclical in nature but mainly due to current steam turbine power plants being used to meet the demand when renewable productions drops. These steam turbines would have to adapt the cyclical nature of the renewable energy sources.

Flexibility, though, is not a simple one-type attribute. It can instead be seen as a spectrum of different attributes categorized by its response time, from practically instantaneous to

long-term, yearly response times. Flexibility can then be categorized in five major types, namely:

1. Spinning reserve and load following
2. Short-term reserve
3. Ramping
4. Daily balancing
5. Seasonal balancing

Out of these five, ramping and seasonal balancing is the two that will be most affected of an increased introduction of renewable compared to a nuclear or fossil fuel based system.[13] The need for ramping can most prominently be showed with the so-called "California duck curve":

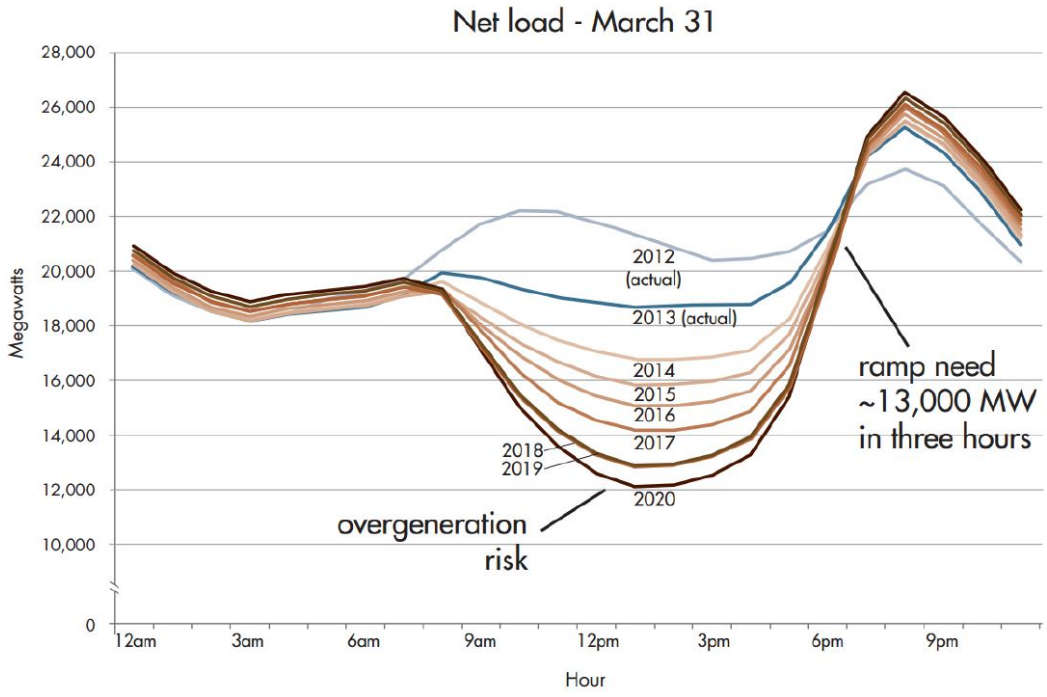

Figure 2.8
The California duck curve[14]

This is a famous case from the state of California showing the total electricity demand minus the solar and wind production, it also points out the possibility of over-generation, due to an inability to ramp down power production. The decreasing solar production combined with the increased demand during the evening hours creates an extreme ramping need that has to be met with some sort of flexible, dispatchable power generation. This will in most cases

fall upon the steam turbine facilities already in use. While this is an extreme case where the demand increases and production decreases almost simultaneously, it could very well be close to reality in most developed countries with a high penetration of renewable energy production in the near future. [14] The new generation of steam turbines designed to tackle this problem would not only have to have very high efficiency during all types of operation but would also have to be much more flexible in their operation compared to previous iterations. This seems to be the most difficult obstacle facing the industry today.

Chapter 3

Steam Turbine Thermal Transient Model

Turbine stresses and in turn the degradation of life time in the turbine derives from the thermal transients in the material. During a transient start-up operation an uneven temperature distribution would be created. Without a sufficiently accurate model, predicting the temperature distribution would be very difficult and therefore a model was developed at KTH, named Steam Turbine Thermal Transient Model (ST3M).

The model uses the program COMSOL and its coupling with MATLAB, with the code being written in MATLAB and calling COMSOL to execute the finite element calculations. ST3M creates a 2D axisymmetric modular geometry modeled after the turbines studied and calculates the metal temperature distribution in the turbine and other thermo-mechanical properties like thermal stresses and thermal induced expansion. ST3M consists of four main sub-models:

1. Steam expansion model - Calculates the temperature and mass flow of the live steam
2. Gland steam sealing model - Calculates the gland coefficients and steam flow through the glands
3. Heat transfer calculations - Either calculates HTCs from theoretical correlations or adjusts HTCs provided by the manufacturer
4. Finite element thermo-mechanical model - Calls COMSOL to handle the finite element calculations and determines the temperature distribution and other thermo-mechanical attributes

The flow chart of the model can be shown in Figure 3.1, where the white boxes indicates calculating steps with no user input. The skewed rectangles indicates user inputs where the yellow ones are determined by design factors usually provided by the turbine manufacturer and the green ones relates to operational decisions.

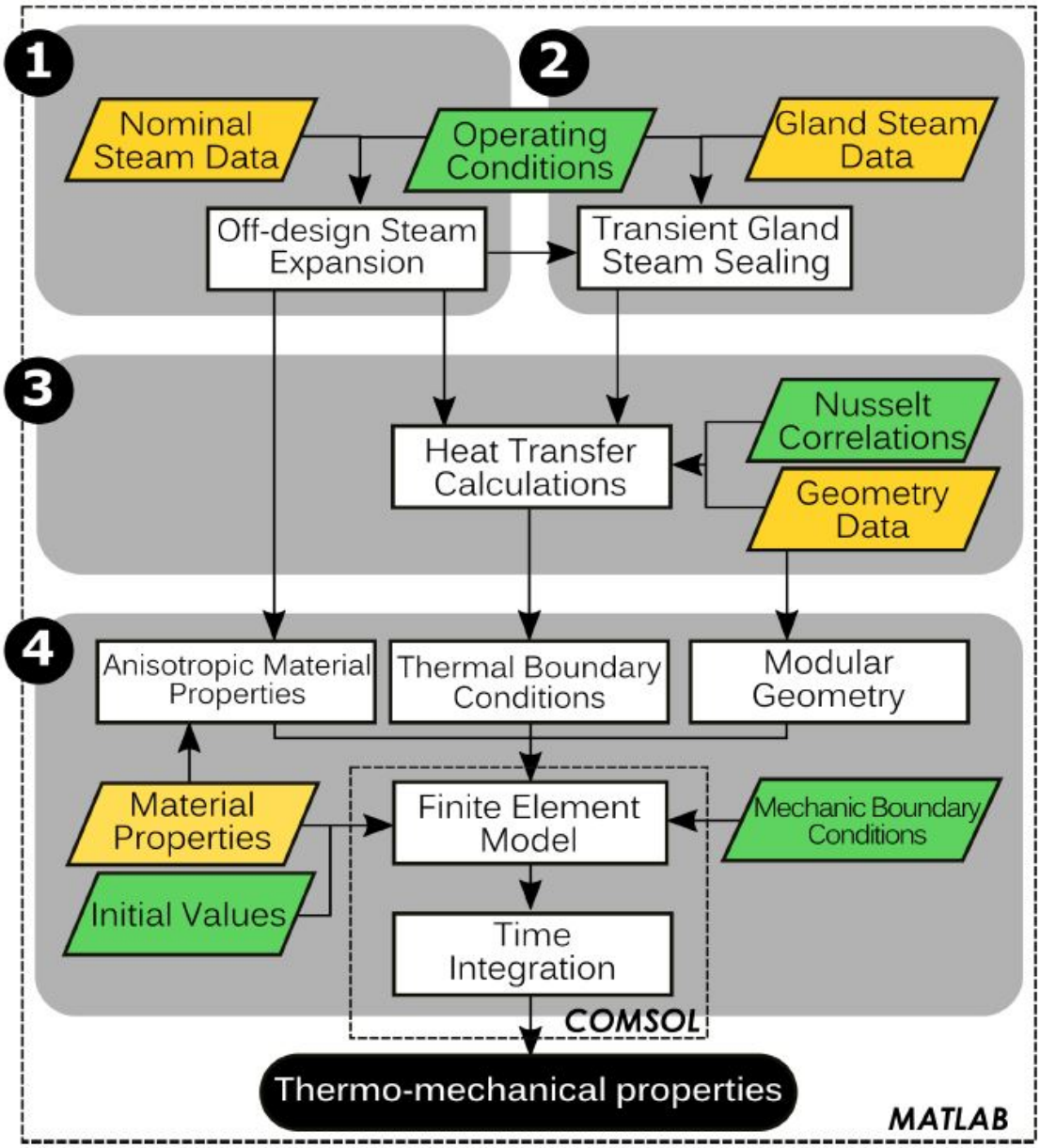

Figure 3.1
ST3M flowchart

The inlet variables are written by the user in a seperate text file that is then read by the code, the variables are: time step, rotational speed of the rotor, inlet pressure, inlet temperature and overall load on the turbine. These are the values that are entering the turbine directly and there is no inlet valve modeled in the code, this will lead to some problems later on. Between

the assigned time steps the code interpolates the other values (load, temperature, pressure and speed). This makes the indata file quite easy to assemble but also gives quite a bit of control over the operation of the turbine.

t	N	load	T	P
0	0	0	0	0
11	3000	100	350	60

t	N	load	T	P
0	0	0	0	0
1	3000	100	350	60
11	3000	100	350	60

Figure 3.2
Simplified example of inlet data

The above picture is an example of two simplified inlet data files but shows an important difference as well. The first data group would simply ramp up the turbine from the initial zero values in 11 minutes, while the second case would ramp up to the same values in one minute and then keep running at the maximum values for an additional ten minutes. It is important to realize that every line of inlet data in the text file represents one data point and that the code interpolates between these points.

3.1 Steam expansion model

The steam expansion model calculates the mass flow and live steam temperature of the turbine during off design operation to later be used in calculating the heat transfer coefficients. The properties calculated uses the inlet conditions which are required to be presented as input data. The remaining off-design properties are calculated using Stodola's eclipse law.

Stodola's eclipse law relates the mass flow coefficient, ϕ, as is defined in equation 3.1 with the pressure ratio across the stage group of the turbine.

$$\phi = \dot{m}\sqrt{\frac{v}{P}} \tag{3.1}$$

In a multistage turbine with a fixed back-pressure and several extraction points the expansion in the turbine can be considered as a single nozzle. This yields the elliptical proportionality of equation 3.2:

$$\phi \propto \sqrt{1 - \left(\frac{P_{in}}{P_{out}}\right)^2} \tag{3.2}$$

This can be rewritten as a ratio between off-design mass flow coefficient and design mass flow coefficient, to eliminate the need for a proportionality coefficient. In equation 3.3 subscript D refers to the design set, which can be set as one of the operating points provided by the manufacturer.

$$\frac{\phi}{\phi_D} = \frac{\sqrt{1 - \left(\frac{P_{in}}{P_{out}}\right)^2}}{\sqrt{1 - \left(\frac{P_{D,in}}{P_{D,out}}\right)^2}} \tag{3.3}$$

Equation 3.3 can be rewritten as:

$$P_{in} = \frac{P_{out}}{\sqrt{1 - \phi^2 Y_D}} \tag{3.4}$$

Where:

$$Y_D = \frac{P_{D,in}^2 - P_{D,out}^2}{P_{D,in}^2 \phi_D^2} \tag{3.5}$$

Equation 3.4 and 3.5 together gives the possibility to calculate the pressure levels throughout the turbine starting with the fixed back-pressure, which is why a turbine's pressure is built "backwards". [15] Since the pressure levels are known in the ST3M code the same equations are used to calculate the mass flows in the different turbine sections. Stodola's eclipse law is also presented in figure 3.3, which shows the relation between initial pressure P_{01}, outlet pressure P_{21}, and flow rate $\dot{m}_{01}$.

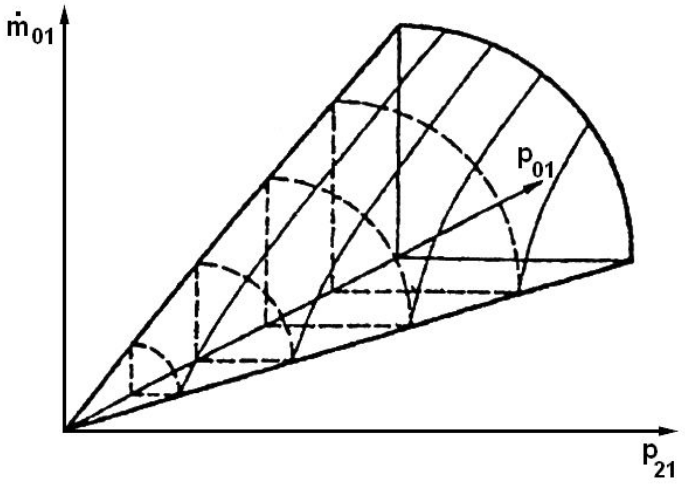

Figure 3.3
Stodola's elliptical cone

The Stodola law only applies for expansion under adiabatic conditions however. This is not the case and therefore the isentropic efficiency needs to be calculated. The isentropic efficiency of the steam expansion is calculated with equation 3.6. $\eta_{s,0}$ is the nominal isentropic efficiency, N is the off-design rotational speed and Δh is the off-design enthalpy difference. The subscript "0" denotes the nominal operational values of the same properties.

$$\eta_s = \eta_{s,0} - 2\left(\frac{N}{N_0}\sqrt{\frac{\Delta h_{s,0}}{\Delta h_s}} - 1\right)^2 \tag{3.6}$$

All of these steam properties together with the efficiency are later used as input into the gland steam sub-model as well as in the heat transfer calculations. The conductivity will be used in the definition of the anisotropic material properties of the inner parts of the turbine. The mass flow will be used together with the steam temperatures to help define the boundary conditions in the blade passage of the turbine.

3.2 Gland steam sealing model

In the studied turbine and all turbines previously studied utilizing the ST3M code, labyrinth gland seals has been used to stop external air from leaking into the system and also stop internal steam leaking out. One labyrinth seal is located at each end of the rotor shaft and works in the way that it creates a long and, for the steam, hard to maneuver channel made up of many teeth. The steam expansion in the seals is a case of throttling with alternating wide

chambers and narrow passages in the labyrinth seals. The steam speeds up in the narrow passages and is then slowed down and dissipates heat in the wide chamber, all while keeping the same enthalpy but lowering the overall pressure. This limits the amount of steam that will leak out from, but it will never be able to eliminate it completely. [16]

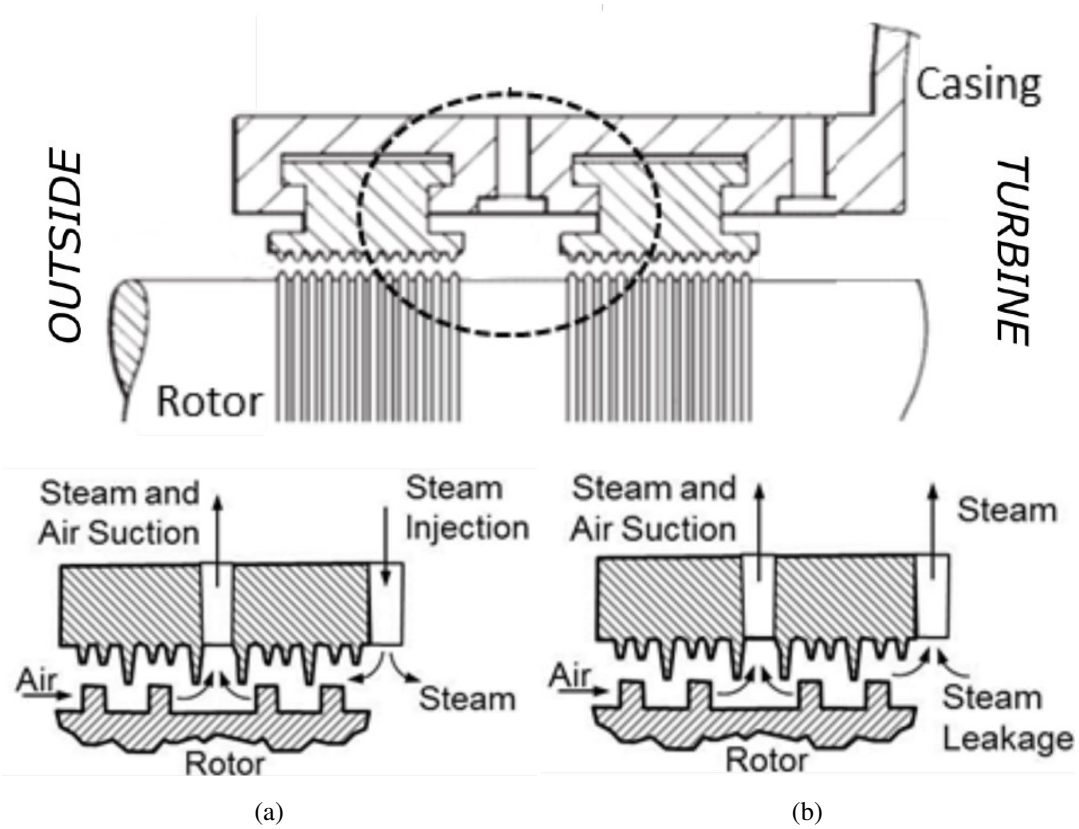

(a) (b)

Figure 3.4: Labyrinth seal showing (a) Externally supplied steam for low load operation and (b) Internally supplied steam for high load operation with excess steam diverted[7]

To take care of the inevitable leakage, and at the same time ingression of air, the steam-air mixture is sucked out with the use of a sub-atmospheric pressure. This requires a constant flow of steam to supply the seal, which creates two distinct modes of operation. When the turbine is running and has a high load, the system is self sustained by the leakage steam from the inlet and outlet section of the turbine. During start up and low load operation the leaking steam is not enough to sustain the needed steam flow for the sealing to properly function, so external steam is required. There's of course not an immediate switch between these two different modes but a transition phase, most commonly the sealing is completely self sustained at 40-60% turbine load.

The mass flow through the seals can be calculated with Equation 3.7 together with Equation 3.8. Where in Equation 3.8 d_s is the seal diameter, δ is the clearance, z is the number of

teeth, τ is the tooth pitch and λ is the tooth width.

$$\dot{m}_{leak} = C_{seal}\sqrt{\frac{P_{in}}{v_{in}}}\sqrt{1-\left(\frac{P_{in}}{P_{out}}\right)^2} \tag{3.7}$$

$$C_{seal} = \frac{\pi \cdot d_s \cdot \delta \cdot K_s(\delta,\tau,z) \cdot \mu(\delta,\lambda)}{\sqrt{z}} \tag{3.8}$$

3.3 Heat transfer calculations

The main objective with the ST3M code is to calculate the temperature distribution in the turbine. The heat transfer model is based on the heat diffusion equation in solids. with r being the radial direction, ϕ the circumferential and z the axial.

$$\frac{1}{r}\frac{\partial}{\partial r}\left(k \cdot r\frac{\partial T}{\partial r}\right) + \frac{1}{r^2}\frac{\partial}{\partial \phi}\left(k\frac{\partial T}{\partial \phi}\right) + \frac{\partial}{\partial z}\left(k\frac{\partial T}{\partial z}\right) + \dot{q} = \rho \cdot C_p\frac{\partial T}{\partial t} \tag{3.9}$$

One characteristic with ST3M is its simplification to a 2D axissymmetric geometry. This simplifies Equation 3.9, eliminating the need for a circumferential dimension and also reduces the calculation time significantly. Still, a finite element method approach is needed to solve the distribution.

3.3.1 Modular geometry and material properties

ST3M was implemented with a modular geometry approach. This allows for any present-day and future turbine to be modeled. The simplification to a 2D axissymmetric geometry is a major one and whilst a steam turbine consists of a complex geometry which is not fully axissymetric, with flanges, inlet piping and the like, it is still fundamentally true.

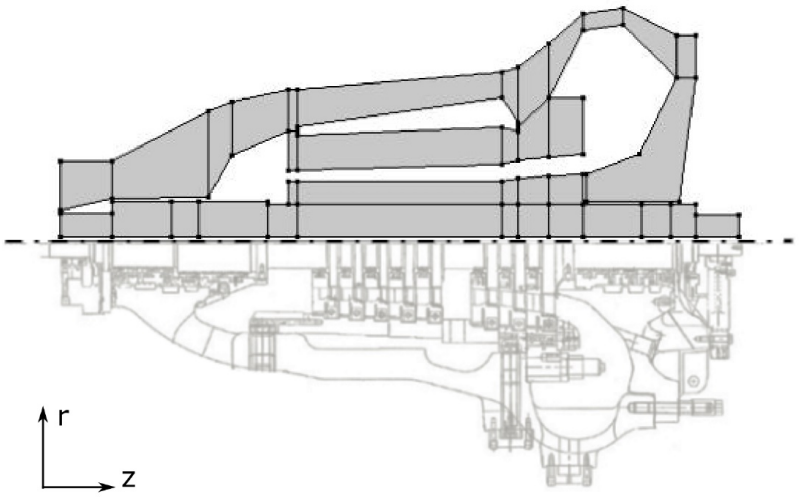

Figure 3.5: Modular geometry

The geometry is divided into four different domains: casing, rotor, diaphragms and discs. The casing and rotor are modeled as isotropic materials, ie equal heat conduction in both axial and radial direction. The diaphragms and discs on the other hand were implemented as anisotropic domains with preferential conduction in the radial direction. This is due to the very complex geometry at these locations with gaps and clearances in between the turbine blades. This is realised with Equation 3.10 and 3.11

$$k_{radial} = \epsilon \cdot k_{steam} + (1 - \epsilon) \cdot k_{metal} \tag{3.10}$$

$$\frac{1}{k_{axial}} = \frac{\epsilon}{k_{steam}} + \frac{1 - \epsilon}{k_{metal}} \tag{3.11}$$

3.3.2 Boundary conditions

For the finite element model to be able to solve the heat conduction equation, boundary conditions needs to be applied throughout the model. There is three types of conditions for a heat transfer process: fixed surface temperature, fixed heat flux at the surface or convection with a fluid. In this model the last condition is by far the most common, occurring wherever steam is inducted into the turbine. However for the second case, since no steam is introduced into the turbine, the radiation condition replaces the convection one. As for mechanical conditions there is simply one: whether the geometry is fixed in space or not. All of these boundary conditions needs to be applied during different time ranges depending on the operation of the turbine, live steam is for example not introduced in the turbine during cool

down. Table 3.1 shows the application for the first, daily operation case. The third case has a similar application of the boundaries as the first one.

Boundary Conditions	Pre-warming	Rolling up	Loading	Nominal Operation	Unloading	Rolling down	Cool-down
Bearing Oil	X	X	X	X	X	X	X
Gland Steam	X	X	X	X	X	X	X
Live Steam		X	X	X	X	X	
Radiation							X

Table 3.1: Application of boundary conditions for daily operation case

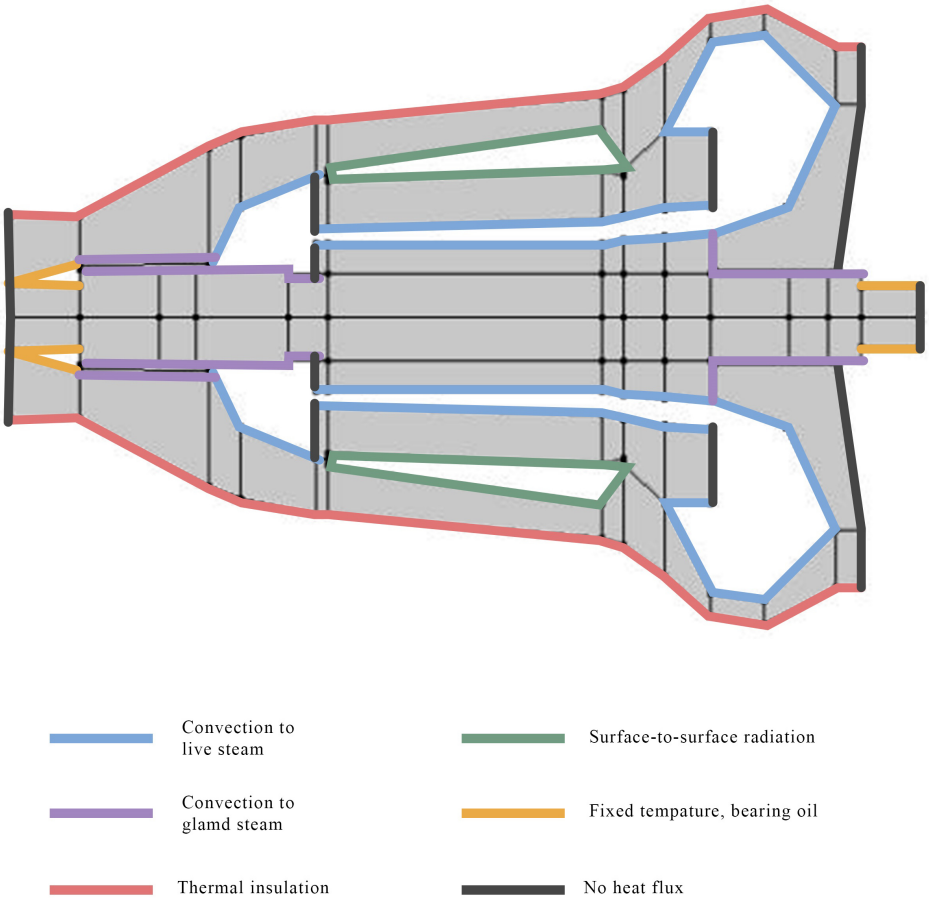

Figure 3.6: Heat transfer boundary conditions for daily operation case

Convection to gland steam The mode of the glands (self sustained or externally supplied) is handled by the code automatically during the operation of the turbine. However when running a long cool down the vacuum of the turbine can be broken and air be allowed to leak in through the gland seals, this was not done in any of the cases studied here though. During the operation of the first two modes the convection boundary condition is active and, if a cool down is studied, is turned off at a specific time step (usually about 5-10 hours after unloading the turbine). Due to the difference in leaked mass flow in the different parts of the labyrinth seals, different HTCs were needed. This was handled by splitting the gland seals in different sections and assigning them different HTCs. The HTC for the gland seals were calculated using equation 3.12 where H is the height of expanding steam and δ is the radial clearance.

$$Nu = 0.476 \cdot \left(\frac{H}{\delta}\right)^{-0.56} \cdot Re^{0.7} \cdot Pr^{0.43} \tag{3.12}$$

Bearing oil The boundaries related to the bearings are determined with a fixed temperature boundary condition. This is active during all of the operation of the turbine. Relatively cold oil is introduced to the bearings but as the transient commences the temperature is assumed to increase dependent on the square of the rotational speed, due to the increase in friction. Still, the oil cannot get too hot and common industrial practise is to cool the oil when the temperature reaches a set value as to avoid kindling temperature. This leads to a lower and upper temperature limit on the oil being introduced.

$$T_{oil} = T_{oil}^{OFF} + \left(T_{oil}^{ON} - T_{oil}^{OFF}\right) \cdot N^2 \tag{3.13}$$

Thermal insulation The casing of all turbines are insulated with some sort of insulating material. This is a cheap, permanent way to keep the turbine innards warmer for longer. However the insulation is not directly represented in the geometry but is instead implemented in the ways of combining the convection to ambient air and heat conduction through the insulating layer. Equation 3.14 shows the way this is achieved, where t_{ins} is the thickness of the insulating layer, k_{ins} is the heat conduction of the insulating layer and HTC_{NC} is the heat transfer calculation related to non-insulated natural convection, this has been set to 8 $\frac{W}{m^2 \cdot K}$. [7]

$$HTC_{ins} = \left[\frac{t_{ins}}{k_{ins}} + \frac{1}{HTC_{NC}}\right]^{-1} \tag{3.14}$$

Convection to live steam The convection in the area affected by the live steam is active during the rolling up and down, loading and unloading as well as the full load operation phase. The ST3M code can handle HTCs both provided by the manufacturer and if they

are not available, can calculate appropriate ones itself. The HTCs in the diaphragms were calculated with equation 3.15 where the characteristic length and flow velocity are in the axial direction. The HTCs in the discs on the other hand were calculated with equation 3.16 where the radius and rotational speed are the characteristic length and speed, respectively.

$$Nu = 0.036 \cdot Re^{0.8} \cdot Pr^{0.333} \tag{3.15}$$

$$Nu = 0.027 \cdot Re^{0.8} \cdot Pr^{0.6} \tag{3.16}$$

If values are given by the manufacturer these would be the HTCs given for nominal operation, since ST3M handles transient operation as well this needs to be addressed. The nominal values are translated to off-design ones using equation 3.17, which is based on the proportionality of the HTCs to $Re^{0.8}$ which in turn makes them proportional to $\dot{m}^{0.8}$.

$$\frac{HTC_{off}}{HTC_{nom}} = \left(\frac{\dot{m}_{off}}{\dot{m}_{nom}}\right)^{0.8} \tag{3.17}$$

Radiation During cool-down when no convection of live steam occurs, surface-to-surface radiation replaces the boundary condition instead. In the cavity in the top part of the turbine radiation is active during all operation. There is a small amount of gland steam entering the turbine but i is not large enough to affect the load of the turbine in a meaningful way. Radiation is determined to occur between the hot metal parts inside the turbine and its emissivity is set to 0.8.

Mechanical boundary conditions There is really only one attribute related to the mechanical side of the boundary conditions, and that is if the boundary is fixed in space or is allowed to move freely. In the radial direction the axissymmetric axis of the rotor was fixed, and in the axial direction it was fixed at the journal bearing on the inlet side. The casing was fixed at its supports in the radial direction on both the inlet and exhaust side, while being fixed in the axial direction only on the inlet side.

Ventilation and friction Ventilation is a phenomenon that occurs in the blade passage of the turbine at low mass flows. The steam flow instead of going through the blade passage, creates small eddies of stagnant steam flow behind each rotor stage. Shown in Figure 3.7.

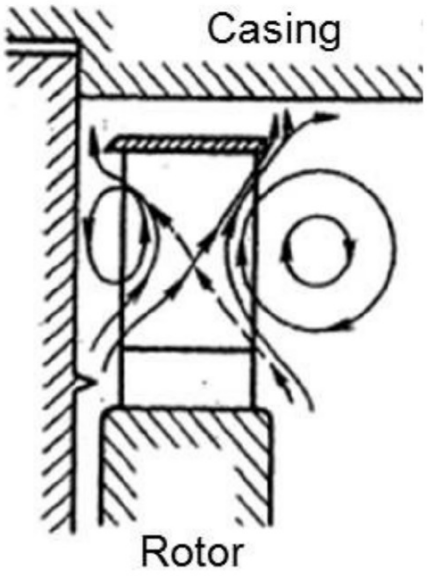

Figure 3.7: Steam path during ventilation

This creates heat spots after every stage and leads to the normal issues associated with higher temperatures, primarily thermal expansion. With enough ventilation the rotor blades can get hot enough to cause rubbing in the diaphragm which leads to excessive damage. This is what causes the thermal expansion in the FSNL case and leads to the radial rubbing and damage on the turbine. It is possible to approximate the generated heat from ventilation with Equation 3.18 and 3.19.[17]

$$W_v = \pi \cdot C \cdot \rho \cdot u^3 \cdot l_{blade} \cdot D_m \tag{3.18}$$

$$C = \left[0.045 + 0.58 \cdot l_{blade/D_m}\right] \cdot \sin \beta_2 \tag{3.19}$$

There is similarly an approximation to calculate the heat generated by the friction, which is shown in Equation 3.20 and 3.21. [16]

$$W_f = \frac{1}{2} \cdot K_f \cdot \rho \cdot u^3 \cdot {D_m}^2 \tag{3.20}$$

$$K_f = 2.5 \cdot 10^{-2} (2s/D_m)^{1/10} \cdot {Re_u}^{-1/5} \tag{3.21}$$

3.4 Finite element thermo-mechanical model

All of the Finite element calculations are handled by COMSOL. The boundary conditions are applied on its previously determined locations. The different materials are implemented in the correct sections. The initial temperature distribution was set as uniform at 365°C. With all the inputs the temperature distribution can be calculated.

Chapter 4

Results

Different versions of the ST3M code was provided, a newer version for another IP turbine and an older, geometrically similar HP turbine. The newer IP version of the code was modified to be able to use with an HP turbine instead. Whilst fundamentally similar in structure, many details needed to be adapted not only to be able to operate the code for an HP turbine but also for the different cases to be studied. For example, an IP turbine always operates against the condensing pressure whilst an HP turbine has a dynamic back-pressure. A large part of work of the thesis consisted of understanding and implementing the new version of the ST3M code.

4.1 Daily Operation Case

As an introductory and validating case real-world data from a CSP plant with a power tower setup was gathered. The cool down time on this data set was limited so it was complemented with industrial cool down curves. The data set was real-world, measured data and was therefore "true to life" while the cool down curve was approximated based on both theory and real-world data. The ST3M model was used to run a case with same inlet data as the data set and then left to cool down for an extended period and was then compared to both the data set and cool down curve. The ambient temperature of the day was gathered and averaged during the whole operating time.[18]

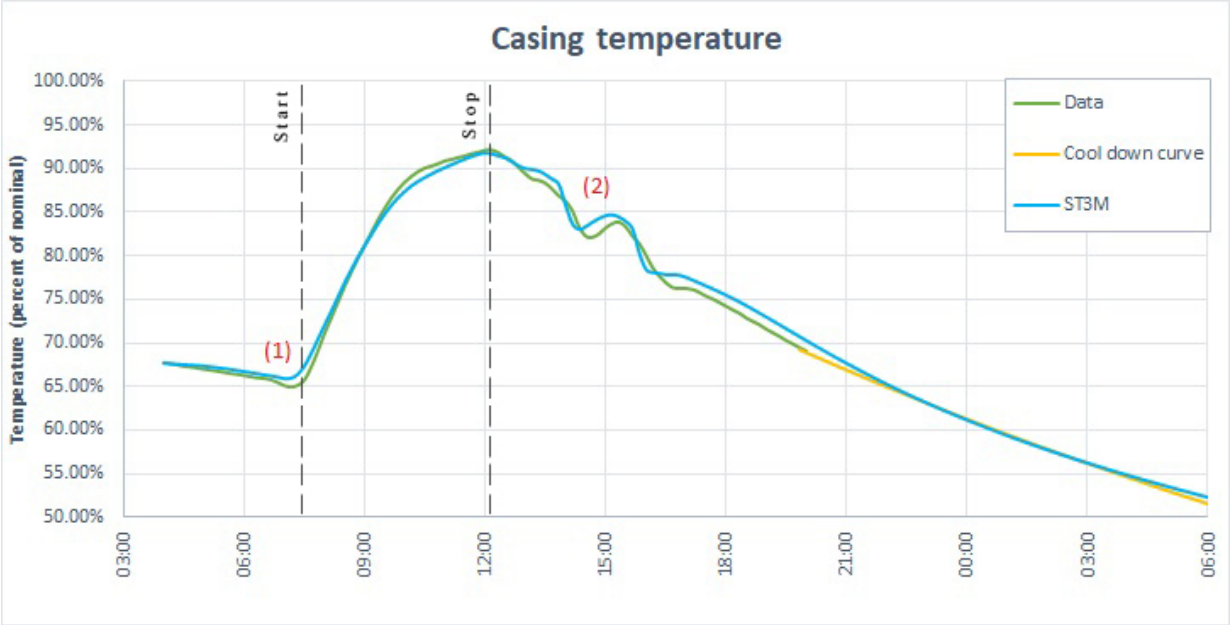

Figure 4.1
Casing temperature, close up on operational time

The relative error between the measured temperature and calculated temperature is shown in figure 4.2.

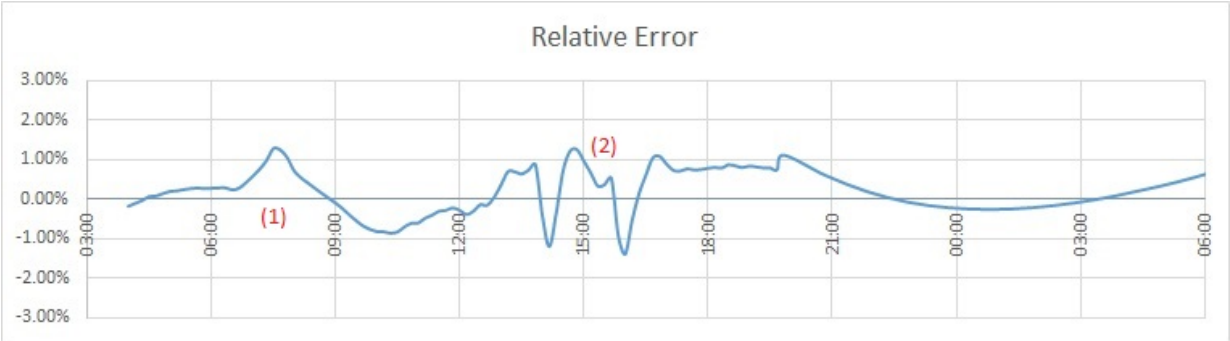

Figure 4.2
The relative temperature error over time, close up on operational time

The model can be seen to follow the real-world data quite well with a few exceptions, most of these however have an explanation. The first dip in the real world data, just before loading (1), is due to the power-plant's setup in using gland steam provided by several different sources. The dip occurs because the gland steam at this moment switches to be provided by a temporarily colder source, which the model does not account for. ST3M has a fixed temperature for the gland steam temperate and it was decided that the relative error was

insignificant and that the focus should lie elsewhere due to the nature of the thesis focused on evaluating rather then developing of the code.

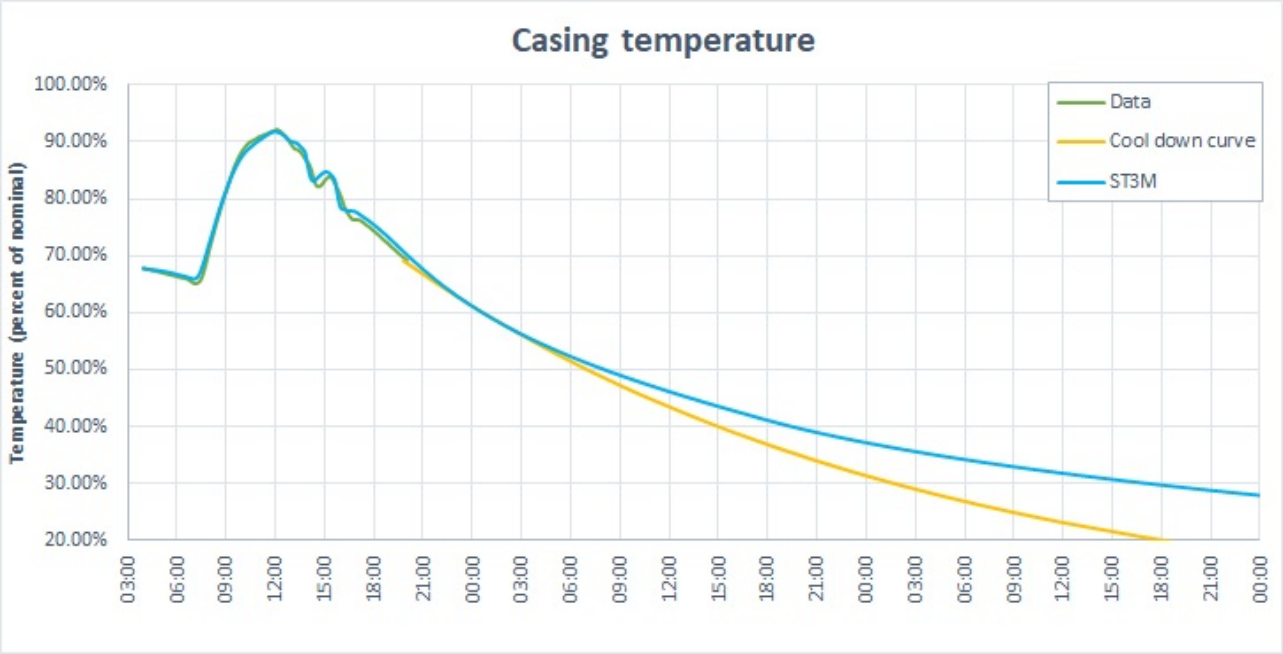

Figure 4.3
Casing temperature, long cool-down

The steep positive and negative gradients during unloading is the cause for the biggest error when comparing to the real-world data (2). This can be explained by the throttling of the inlet valve. The real-world data is measured before the valve while the model attributes are the inlet conditions into the turbine. As long as the inlet valve is fully opened this does not pose a problem, but when the valve is throttled to maintain the pressure, the temperature will drop which is not considered in the model. The inlet temperatures at these time steps therefore had to be manually adjusted to simulate the temperature drop over the valve.

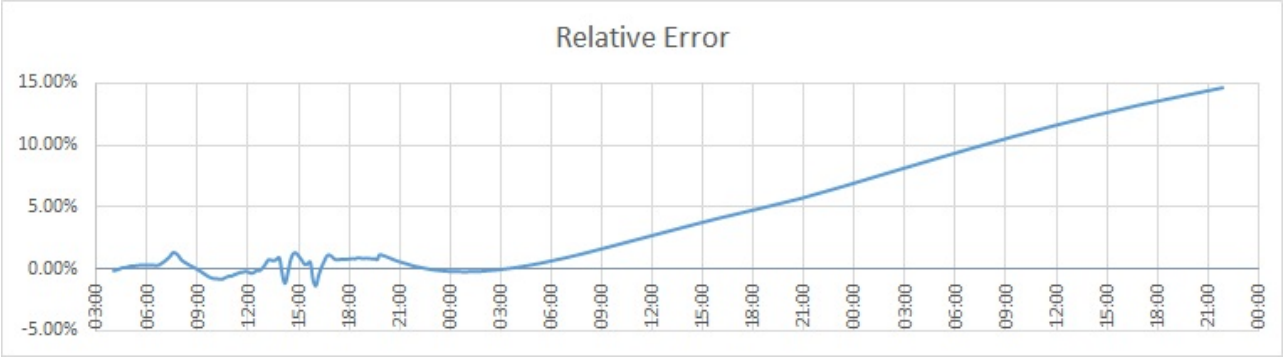

Figure 4.4
The relative temperature error over time, long cool-down

Compared to the cool-down curve the model also corresponds quite well early on. Up until 06:00 the following morning it corresponds very well, staying under 1% relative error. However, the model starts to diverge from the cool-down curve quite rapidly, which means the error will increase for longer cool-down periods. 06:00 the next day the relative error has already reached almost 10 % and will continue to increase to 15% during the studied period. Several parameters was varied to try to reduce this divergence, both related to the ST3M tool but also in the cool down curve as well. This was unsuccessful and the best result is what is presented. The reason for the divergence was never resolved and the best reasoning as to why it happened is that there exist a difference in assumptions between the cool down curve and the ST3M tool. Due to the diverging results the model would be unfit for anything longer than a nightly stop of the turbine,. However for daily cyclical plants, the model will work very well with the caveat that the user needs to manually adjust the temperature for some time steps.

4.2 Full Speed, No Load Case

The second case was also a validating case in a way, the real world situation was that a geometrically similar turbine to the one previously studied incorrectly entered a state of full speed with no load (FSNL), with close to no mass flow through the turbine. This caused excessive ventilation and caused huge radial rubbing due to thermal expansion in the turbine. This is what was attempted to be replicated with the model. The geometry was unaltered since both the turbines was geometrically similar, the new turbine essentially being a smaller scaled version of the first case one. The boundary conditions remained the same as previously but their application time was adjusted to fit the new case. Mainly the convection was replaced during the studied period of FSNL with radiation instead. The glands were assumed to still be provided with steam, so the convection condition for the glands were kept.

The model was run in a nominal state at first to obtain a somewhat realistic temperature distribution in the turbine before being unloaded and entering the FSNL-state. The actual

operational data before the accident was not available so therefore the nominal operation was used. When the turbine was unloaded the ventilation and friction boundary condition was applied, the ventilation work distributed evenly on both sides of the blade passage and the whole friction work was applied to the rotating side of the blade passage.

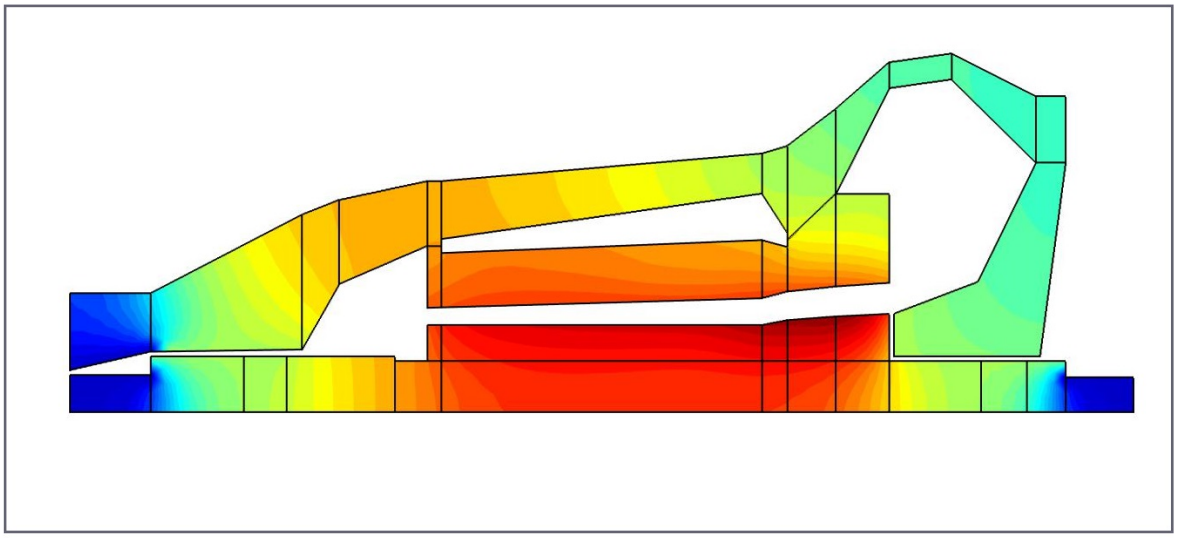

Figure 4.5
Temperature distribution after 1 hour of FSNL

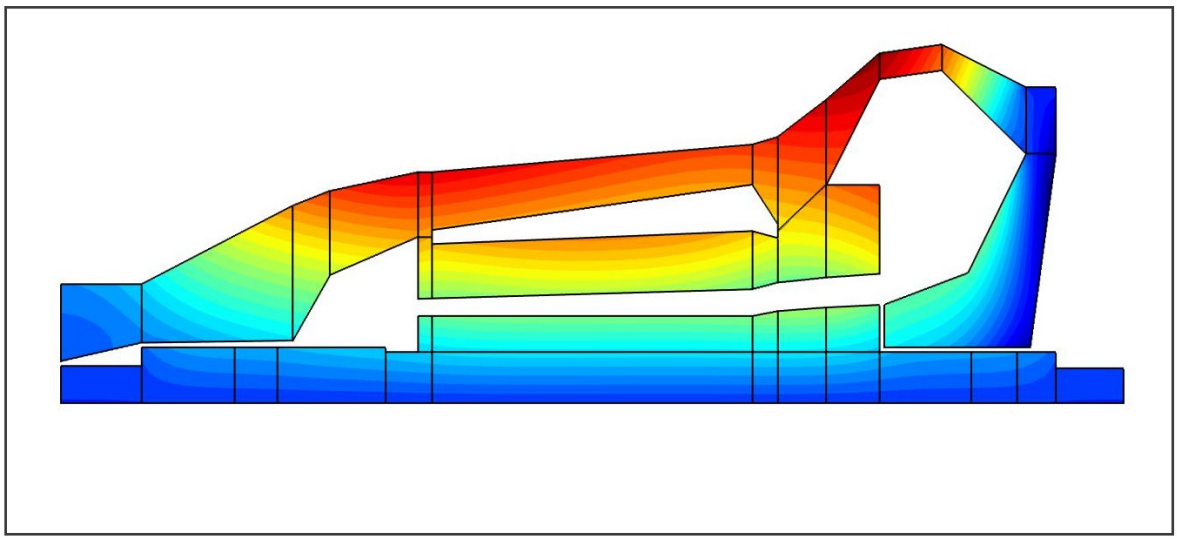

Figure 4.6
Displacement in radial direction after 1 hour of FSNL

Replicating this case was not fully achieved however. The hottest stages was always the stages towards the back of the turbine, the relative differential expansion was also largest at the LP stages. This corresponds with the theory found in [17], where the geometry of the blades are the most influential factor, the longer the blades the higher the ventilation work. The last stage blades (LSBs) are usually the most sensitive blades in respect to ventilation and friction. [3] The close-to-zero mass flow and unusual pressure-distribution in the turbine probably made it difficult to replicate the real-world scenario. The temperatures at the hottest stages was at about the level expected for radial rubbing to take place, although as mentioned it occurred further back than expected.. The high temperatures achieved might have meant that the metal of the blades was so high it entered a state of plastic deformation, something not reproduced in ST3M which might have contributed to the different result.

4.3 Load Drop

Finally, the effects of a sudden load drop and the subsequent load ramping on the turbine was studied. This was simulating the response from a CSP plant when the sun was shaded by a cloud. This leads to lower irradiance from the sun and lower steam production. This is handled by throttling the inlet valve to keep the pressure uniform, but as previously mentioned this causes the temperature to drop which essentially means that the inside of the turbine is forcefully cooled during the load drop. The exact temperature decrease for the specific load drops was provided by Siemens. Both the casing and rotor was measured at three different radii at the same axial location, the surface facing the live steam, the middle of the

component (r=R/2 for the rotor) and the third measurement being the axisymmetric position for the rotor (r=0) and the surface facing the ambient temperature for the casing. This to be able to calculate the temperature difference over the component, where the most interesting temperature difference is the one where the temperature closest to the live steam is compared to the temperature in the middle of the component ie r=R/2 for the rotor. This is because as seen in figure 2.3 at roughly the middle point of the component is where the thermal strain is equal to zero. The temperature difference as explained in a previous chapter can be directly related to the thermal stress of the component and is the main restricting attribute for faster starts.

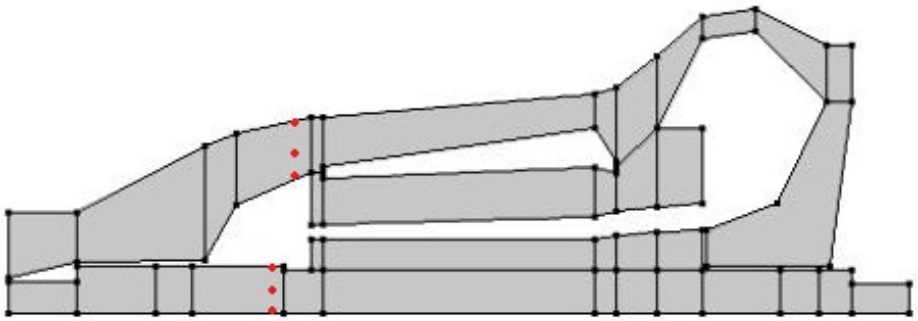

Figure 4.7: Measure points in the rotor and casing

Different load drops, down times and loading rates where studied and the temperature was measured for each case. The load drop is the percentage of loss of power compared to the maximum amount of power output. The down time is the total time that the load drop is in effect, which means that the cooler steam is injected into the turbine for a longer duration and subsequently lowers the temperature of the casing and rotor further. The loading rate occurs after the duration of the load drop and is percantage of maximum output per minute, ie after a 75% load drop it will take 3 minutes to reach maximum power output at a 25% /min loading rate

Load drop:	25%, 50%, 75%
Down times:	2 minutes, 5 minutes, 10 minutes
Loading rate:	2.5%, 5%, 15%, 25%

Table 4.1: Load drop cases

This gives a total of 36 different cases studied, below the temperature and temperature difference for two of the cases is shown. The graphs related to the temperature diffrences were all normalised with regard to the highest achieved temperature difference, which was the negative value during the 75% load drop shown in Figure 4.9 and Table 4.2.

It was found that the lowest negative value for the temperature difference was only dependent on the load drop, the down time and ramp rate naturally did not affect it and is show in Table 4.2 below.

Load Drop	DeltaT Dip
75%	100.00%
50%	58.59%
25%	24.85%

Table 4.2: Load drop dip temperature (percentage of maximum)

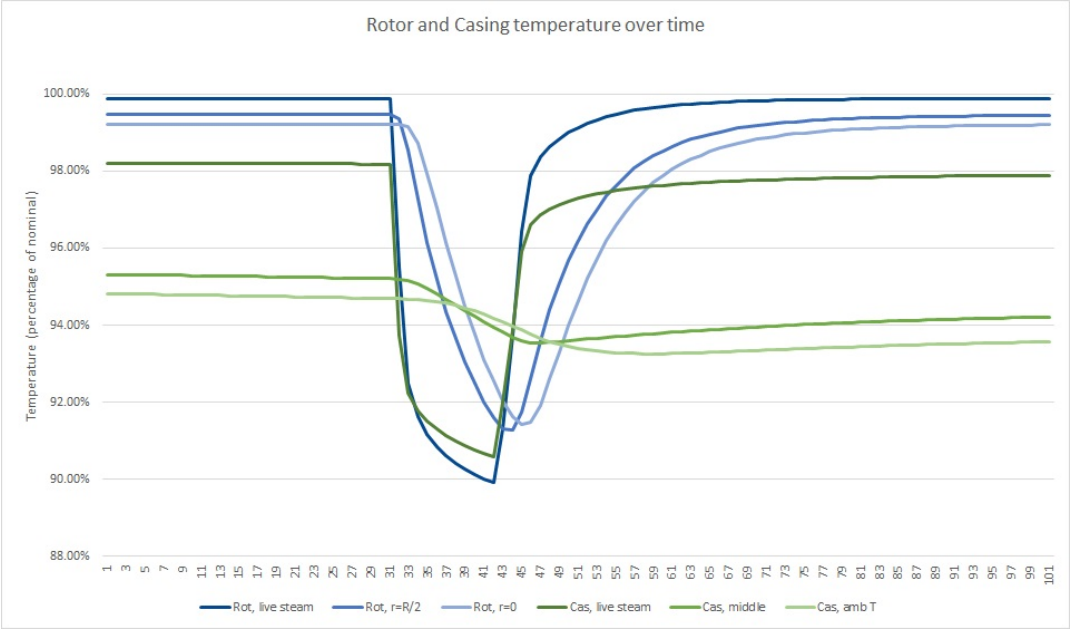

Figure 4.8
Temperature of rotor and casing for 75% load drop, 10 minutes down time and 25% ramping rate.

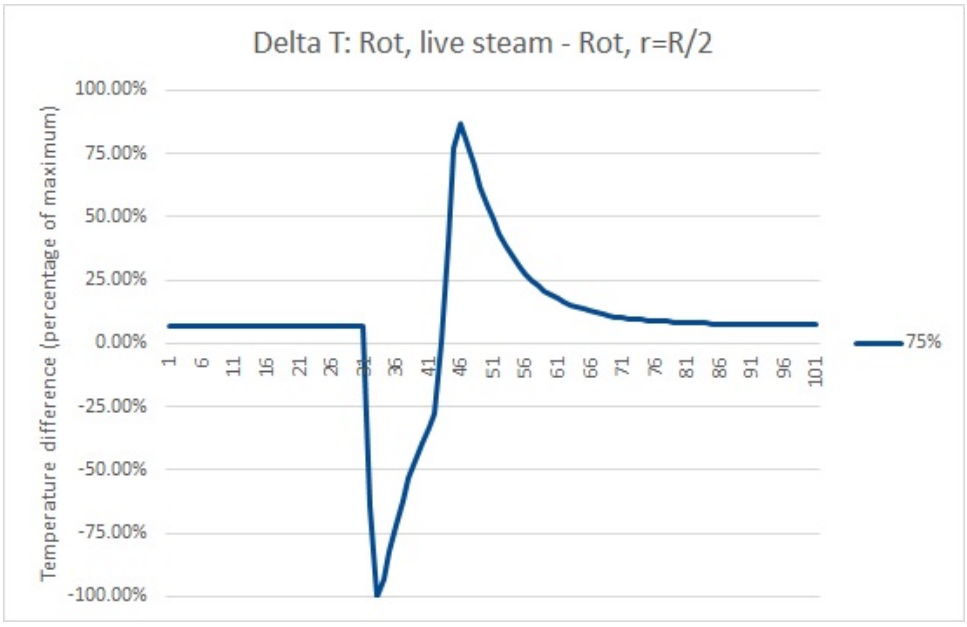

Figure 4.9
Temperature difference of rotor for 75% load drop, 10 minutes down time and 25% ramping rate.

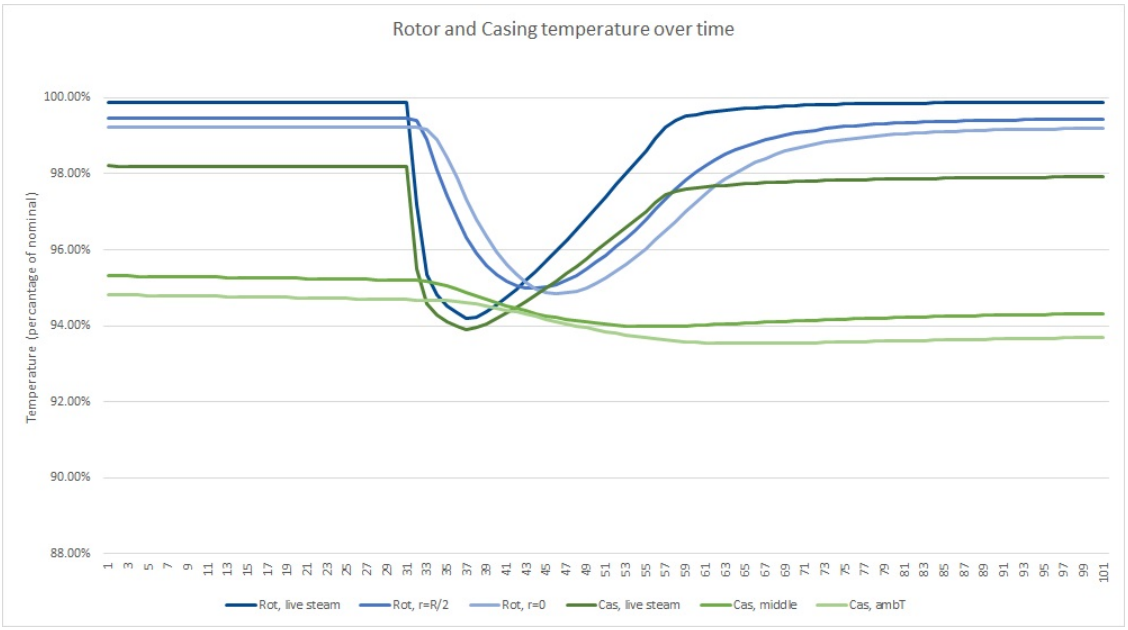

Figure 4.10
Temperature of rotor and casing for 50% load drop, 5 minutes down time and 2.5% ramping rate.

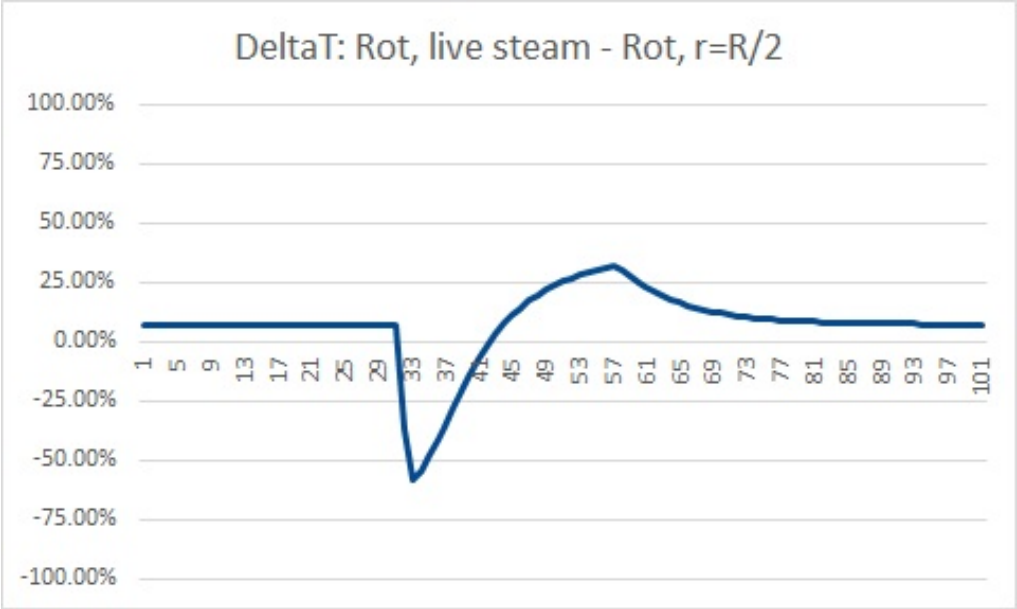

Figure 4.11
Temperature difference of rotor for 50% load drop, 5 minutes down time and 2.5% ramping rate.

The highest positive temperature difference for each case is presented below:

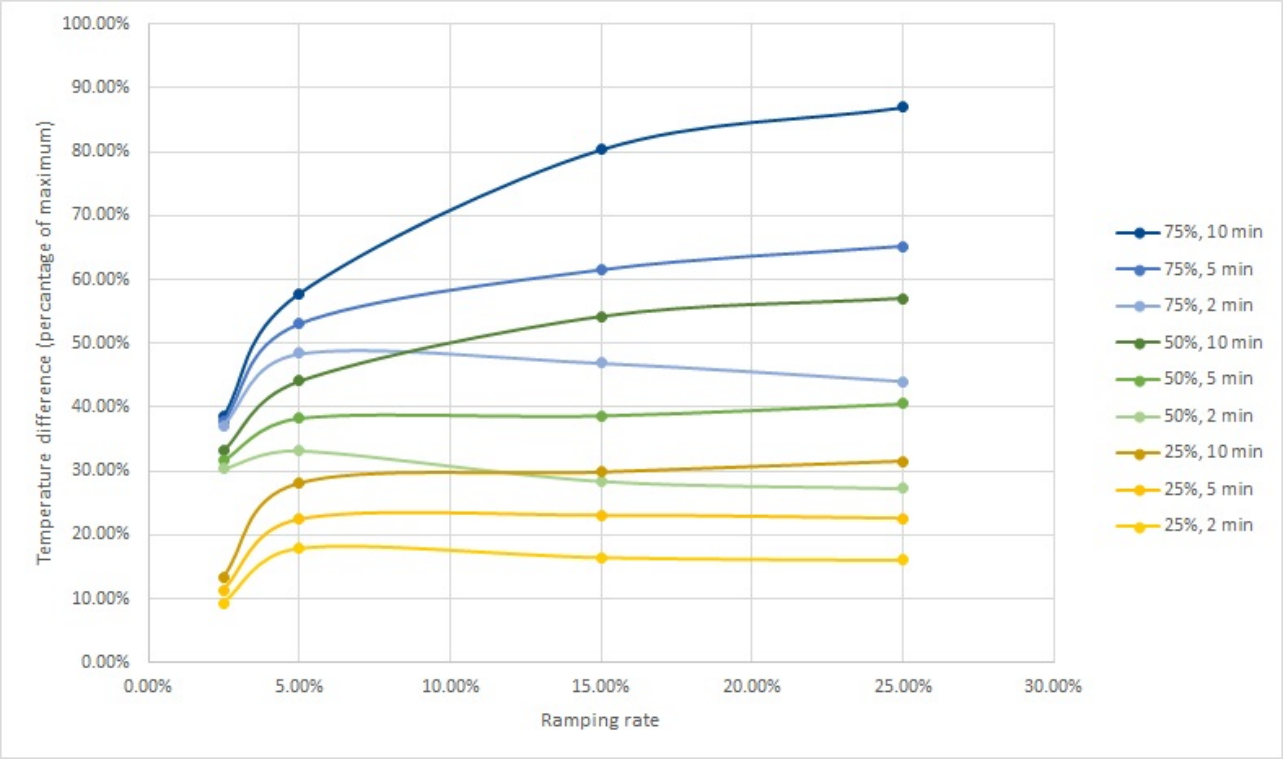

Figure 4.12: Maximum temperature difference reached for each case

It can be seen that ramping rates affect the cases with higher load drop more, for the 25 % load drop it hardly makes any discernible difference at all. For the larger load drops and short down times it can be seen that a quick ramping rate is to be preferred, this can be reasoned to be because the temperature in the middle of the rotor hasn't had time to cool of as much compared to slower ramping rates and to prolong the injection of relatively colder steam serves no purpose, in this case it is instead advantageous to have a faster ramp rate. This is off course also good in the way that the CSP plant will reach its maximum power output more quickly compared to the lower ramp rates. However the absolutely largest factor in the maximum temperature difference is obviously the actual load drop itself.

To find the maximum allowable temperature difference equation 2.1 can be used together with material data and the yield strength in the rotor and casing. This could be done to optimize the ramping after load drops of different magnitudes and thus save important minutes after every load drop. Due to the time limitations of the master thesis there was no time to include it in this paper nor was it researched by Siemens during its duration. However this could be something intersesting to work on in the future. With the help of ST3M one would be able to create a road map of sorts where every case is studied and the allowable temperature difference tracked.

Chapter 5

Discussion and conclusion

In this thesis a 2D FE model based on MATLAB code coupled with COMSOL was studied. A modular axissymmetric geometry of an HP turbine provided by previously studies was used as the base for three different cases of operation.

1. Daily operation with long cool down
2. Full Speed, No Load case with ventilation and friction heat generation
3. Sudden load drop with subsequent ramping to nominal

The two first cases served as validating cases, the first one to see if the model could closely follow the daily operation of a CSP plant with a shutdown for a duration similar to a nightly and weekend shutdown. The relative error was well within an acceptable range during the daily operation but diverged during the cool down which led to large errors for a cool down duration similar to a weekend shutdown. Since both the cool down curve and the ST3M results are theoretical in essence, the difference between them might be different assumptions about the properties of the turbine (the insulation, gland steam temperature etc). Since the problem starts to appear when the measured data ends and the cool-down curve is introduced, this would lead one to believe that there is some disparity between them not considered. Also worth mentioning is that the relative error increases linearly, which furthers supports the idea that there is some parameter that has not been fully considered. During testing this has not been resolved however.

The second case evaluated if the heat generation and differential thermal expansion caused by ventilation work would occur at the same stage as in the real world case. This was not completely achieved however and the reason why has not yet been fully understood. The results in ST3M corresponds to what can be expected from the theory, the most ventilation is developed at the last stages in the turbine. This does not fit with what happened in the actual case, the best reasoning as to why is that there are some characteristics of the operation that was not considered in the model. The precise state of the turbine during this operation may have contributed to the different result. The unusual pressure distribution in the turbine and the low mass flow may have added to the difficulty in modeling the operation and may have caused unknown phenomenas in the real turbine not at all considered. The temperatures

reached was in the region associated with radial rubbing as well as plastic deformation even if the stages did not correspond to what happened in the real turbine, this gives some hope to the utility of the tool and would make it somewhat usable to evaluate the maximum temperature achieved in FSNL operation.

The third case related to sudden load drops and their effect on the life time of the turbine related to maximum achieved temperature difference in the rotor. The main factor impacting the temperature difference was the load drop itself, higher load drops resulted in overall higher temperature differences. Other than that, longer down times always resulted in higher differences. Although this affected the higher load drops more so than the lower load drops. The difference between 10 minutes and 2 minutes down time was 40 percentage points for the 75% load drop compared to only 15 percentage points for the 25% load drop. The ramp rates affected the bigger load drops more in general. For the 10 and 5 minute down time, increasing the ramp rate increased the temperature difference. While for the 2 minute down time the temperature difference actually dropped with higher ramp rates, excluding the 2.5% ramp rate which always was lower than the 5% ramp rate. The temperature difference seems to converge when the ramp rate is set to 2.5%, if the ramp rate would be infinitively slow a minimal value should be achieved no matter the load drop nor down time. These temperature differences that were calculated could be used to optimize the ramping rate after a load drop based on the allowed thermal stress in the turbine. This could not only lead to saving crucial minutes after every load drop, it would also give the operator a greater insight in the life time consumed. Considering the amount of load drops during a plants operational life this could lead to a great amount of extra production for the operator and also contribute to a greater life time which also would save money in the long run.

ST3M has been found throughout the thesis to follow load changes very well and can also be utilized for shorter duration cool downs. It is not however a universal tool capable of handling every sort of case. When a low mass flow was introduced, both in the longer cool down and in the FSNL, the model deviated from the real world data. This might be because something not considered either in the model or some circumstance in the real world. The tool always needs quite a bit of user-input and thought behind it before using it and is not a plug-and-play type of tool. This should not however pose a problem with suitable cases and as experience with the tool increases so should the usability of it. In this study only one type of HP turbine was studied, to be truly usable the whole turbine fleet would need to be modeled and implemented. This would surely take some time but can be done with a needs based approach and once completed will be usable forever.

Bibliography

[1] S.L Dixon. *Fluid Mechanics, Thermodynamics of Turbomachinery*. Butterworth-Heinemann, 1998.

[2] 21st Centyry Tech. https://www.21stcentech.com/technology-steam-turbine-power-plants-increases-efficiency-reducing-co2-emissions/, Last accessed 22 August 2018.

[3] Alexander S. Leyzerovich. *Steam Turbines for Modern Fossil-Fuel Power Plants*. CRC Press, 2007.

[4] Y. Enomoto. Steam turbine retrofitting for the life extension of power plants. In Tadashi Tanuma, editor, *Advances in Steam Turbines for Modern Power Plants*, pages 397–436. Woodhead Publishing, 2017.

[5] Magnus Genrup and Marcus Thern. Ångturbinteknik - årsrapport 2016. Technical report, Energiforsk, Oktober 2017.

[6] Weibull. Miner's rule and cumulative damage models, 2017. http://www.weibull.com/hotwire/issue116/hottopics116.htm, Last accessed 29 May 2018.

[7] Monika Topel. *Improving Concentrating Solar Power Plant Performance though Steam Turbine Flexibility*. PhD thesis, KTH Royal Institute of Technology, 2017.

[8] Monika Topel, Åsa Nilsson, Markus Jöcker, and Björn Laumert. Investigation into the thermal limitations of steam turbines during start-up operation. *Journal of Engineering for Gas Turbines and Power*, 140, 2018.

[9] L. L. Vant-Hull. Central tower concentrating solar power (csp) systems. In Keitgh Lovegrove and Wes Stein, editors, *Concentrating solar power technology*, pages 24+0–281. Woodhead Publishing, 2012.

[10] NREL. https://www.nrel.gov/csp/solarpaces/project_detail.cfm/projectID=62, Last accessed 9 August 2018.

[11] TechXplore. https://techxplore.com/news/2016-09-china-investing-heavily-solar-power.html, Last accessed 9 August 2018.

[12] Jurgen Birnbaum, Jan Fabian Feldhoff, Markus Fichtner, Tobias Hirsch, Markus Jöcker, Robert Pitz-Paal, and Gerhard Zimmerman. Steam temperature stability in a direct steam generation solar power plant. *Solar Energy*, 85(4), 2011.

[13] Brendan Pierpoint, David Nelson, Andrew Goggins, and David Posner. Flexibility, the path to low-carbon, low-cost electricity grids. Technical report, Climate Policy Initiative, April 2017.

[14] Paul Denholm, Matthew O'Connell, Gregory Brinkman, and Jennie Jorgenson. Over-generation from solar energy in california: A field guide to the duck chart. Technical report, NREL, November 2015.

[15] David H. Cooke. Energy incorperated. In *Modeling of off-design multistage turbine pressures by Stodola's ellipse*, pages 205–234, 1983.

[16] Alexander S. Leyzerovich. *Large Power Steam Turbines: Design and Operation*, volume 1. PennWell Books, 1997.

[17] Walter Traupel. *Thermische Turbomaschinen*. Springer-Verlag, 3 edition, 1982.

[18] Western Regional Climate Center RAWS USA Climate Archive. https://raws.dri.edu/cgi-bin/rawMAIN.pl?caCMID, Last accessed 7 June 2018.